Supporting Information

Lee et al. 10.1073/pnas.1307010110

SI Text

Pore Size

The Br density distribution in Fig. 4 shows that the lipidic structure of the melittin pore is consistent with the toroidal model. To resolve the internal diameter of the pore, we need to know the positions of the lipid headgroups, which Fig. 4 does not provide. The electron density distribution of the whole system constructed from F_0 is shown in Fig. S1. The central region, where the pore is located, has too many local high-density regions separated by short distances; it could not be resolved by the small-angle diffraction [this was discussed in detail by Qian et al. (1), who compared a complex structure against a simple structure]. The absence of large-angle diffraction peaks is an intrinsic property of liquid-like unit cells.

The structure in the region outside the pore is nevertheless faithfully reproduced by F_0. Note that individual melittin is invisible by diffraction, because the peptide positions are not correlated from one unit cell to another in a liquid-like continuous structure. The lipid structure is highlighted by the high electron density groups of phosphate (P) and Br and the low electron density methyl region at the ends of the lipid chains. Near the edge of the unit cell, the structure is close to a free lipid bilayer, with the P groups on the surfaces and the chains extending vertically toward the middle. A Br layer is in the middle of each monolayer. One can see that the monolayers are bending toward the pore. The ridge lines of the P peak and the Br peak are shown by white dashed lines. From the edge of the unit cell toward the pore, the P-to-Br distance decreases from 1.4 nm to ∼1.0 nm. From Fig. 4, we measure the Br-Br distance across the pore to be 2.7 nm. Thus, we estimate the internal diameter of the pore to be ∼0.7 nm in the crystalline. This is in a very dehydrated condition. The melittin pores in fully hydrated lipid bilayers were accurately measured by neutron scattering to be 4.4 nm in diameter (2).

Energy Calculation

From Interfacial Binding to Transmembrane Insertion. According to the model of Terwilliger et al. (3) for a membrane-bound melittin helix, the following residues of melittin are exposed to water, whereas the remaining residues are in contact with the apolar region of the lipid bilayer: Lys-7, Thr-10, Thr-11, Pro-14, Ser-18, Lys-21, Arg-22, Lys-23, Arg-24, Gln-25, and Gln-26. We used the free energy scale of Moon and Fleming (4) to calculate the total energy cost of transferring these residues into the bilayer interior: 16.2 kcal/mol = 27 k_BT. If we use the translocon-to-bilayer energy scale measured by Hessa et al. (5), the transfer energy is 22.12 kcal/mol = 37 k_BT.

Elevation of the Chemical Potential of Interface-Bound Melittin. Interfacial binding increases the interfacial area of the monolayer (6). A fractional area expansion, $\Delta A/A$, is a strain whose corresponding stress is the monolayer tension, $\sigma = (K_a/2)\Delta A/A$, where K_a is the bilayer stretch coefficient and $K_a/2$ is the monolayer stretch coefficient (7). Let A_P be the area increase (of the monolayer) by one peptide monomer, which can be calculated from the membrane thinning measurement (Fig. 2), $A_P = 111$ Å^2 (see below). Then the increase of the chemical potential per peptide monomer is $\Delta\mu = (K_a/2)\Delta A/A\Delta A_P$. $K_a \approx 240$ mN/m (7). At $\Delta A/A = 0.034$, $\Delta\mu = 1.1\ k_BT$.

The membrane area expansion per peptide is $A_P \cdot \Delta A/A = -\Delta h/h = (P \cdot A_P)/(L \cdot A_L)$, where A_L is the molecular cross-section per lipid molecule in the plane of bilayer. For a 7:3 dioleoyl phosphatidylcholine to dioleoyl phosphatidylglycerol ratio, the average lipid cross-section is $A_L = 72.8$ Å^2 (8). From $-\Delta h/h = 0.034$ at a 1:45 peptide-to-lipid molar ratio, we obtain $A_P = 111$ Å^2. Note that the value of A_P is considerably smaller than the molecular cross-section of melittin helix (∼400 Å^2) (3). This is understandable because there are water molecules between the lipid headgroups and the binding of melittin might release water molecules from the headgroup region (8). The value of A_P has been shown to vary with the variation of lipid headgroups (9).

Giant Unilamellar Vesicle Protrusion

As explained in the main text, the protrusion length initially increased due to melittin binding at constant giant unilamellar vesicle (GUV) volume (solid diamonds in Fig. 1, before the molecular leakage). This initial protrusion length increase can be precisely converted to the membrane area increase. Once the stable pores were formed in the membrane, the GUV volume was no longer constant. The osmolality of the GUV was controlled by the sucrose solution inside and the glucose solution outside (both at ∼200 mM). As first explained by Longo et al. (10), the finite size of the pores allowed a slightly greater influx of the smaller glucose than the efflux of the larger sucrose. The resultant osmolality imbalance induced a net water influx, causing a volume increase in the GUV. After the melittin binding came to equilibrium, the membrane area was constant. An increasing GUV volume would cause the protrusion length to decrease, as shown in Fig. 1. As a proof of the explanation above, we had exchanged glucose and sucrose. The result was a decreasing GUV volume and increasing protrusion length (11).

1. Qian S, Wang W, Yang L, Huang HW (2008) Structure of transmembrane pore induced by Bax-derived peptide: Evidence for lipidic pores. *Proc Natl Acad Sci USA* 105(45): 17379–17383.
2. Yang L, Harroun TA, Weiss TM, Ding L, Huang HW (2001) Barrel-stave model or toroidal model? A case study on melittin pores. *Biophys J* 81(3):1475–1485.
3. Terwilliger TC, Weissman L, Eisenberg D (1982) The structure of melittin in the form I crystals and its implication for melittin's lytic and surface activities. *Biophys J* 37(1): 353–361.
4. Moon CP, Fleming KG (2011) Side-chain hydrophobicity scale derived from transmembrane protein folding into lipid bilayers. *Proc Natl Acad Sci USA* 108(25):10174–10177.
5. Hessa T, et al. (2005) Recognition of transmembrane helices by the endoplasmic reticulum translocon. *Nature* 433(7024):377–381.
6. Huang HW (2009) Free energies of molecular bound states in lipid bilayers: Lethal concentrations of antimicrobial peptides. *Biophys J* 96(8):3263–3272.
7. Rawicz W, Olbrich KC, McIntosh T, Needham D, Evans E (2000) Effect of chain length and unsaturation on elasticity of lipid bilayers. *Biophys J* 79(1):328–339.
8. Lee MT, Chen FY, Huang HW (2004) Energetics of pore formation induced by membrane active peptides. *Biochemistry* 43(12):3590–3599.
9. Lee MT, Hung WC, Chen FY, Huang HW (2005) Many-body effect of antimicrobial peptides: On the correlation between lipid's spontaneous curvature and pore formation. *Biophys J* 89(6):4006–4016.
10. Longo ML, Waring AJ, Gordon LM, Hammer DA (1998) Area expansion and permeation of phospholipid membrane bilayer by influenza fusion peptides and melittin. *Langmuir* 14(9):2385–2395.
11. Sun Y, Hung WC, Chen FY, Lee CC, Huang HW (2009) Interaction of tea catechin (-)-epigallocatechin gallate with lipid bilayers. *Biophys J* 96(3):1026–1035.

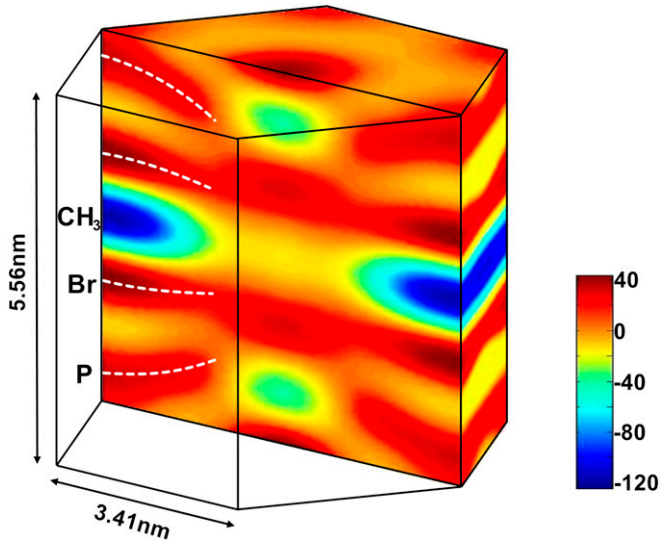

Fig. S1. Electron density distribution of the whole system constructed from F_0, in a unit cell of the R phase, expressed by color on a relative scale. The white dashed lines indicate the ridge lines of the phosphate (*P*) peak and Br peak.

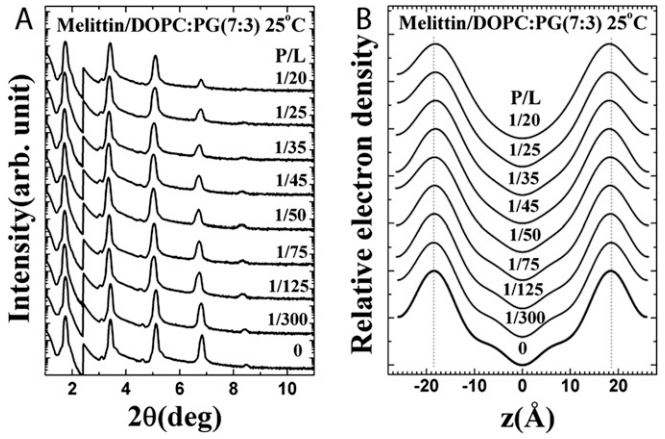

Fig. S2. (*A*) Lamellar diffraction patterns of melittin–lipid (7:3 DOPC/DOPG ratio) multilayers for a peptide-to-lipid molar ratio (P/L) series in full hydration. arb., arbitrary; DOPC, dioleoyl phosphatidylcholine; DOPG, dioleoyl phosphatidylglycerol. (*B*) Diffraction data were converted to the electron density profile of one repeating unit (i.e., a bilayer) for each P/L. The density peak on each side is that of the *P* group. The phosphate peak-to-phosphate peak (*PtP*) distance across the bilayer as a function of the P/L is shown in Fig. 2.

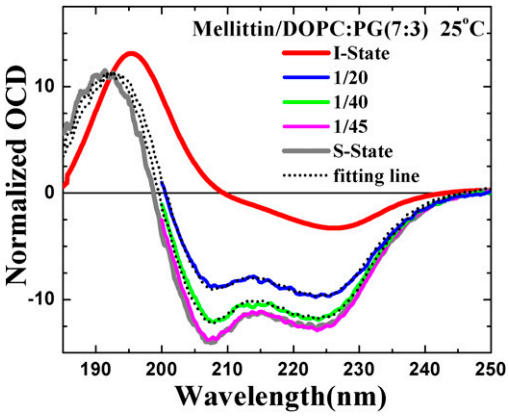

Fig. S3. Oriented circular dichroism (OCD) of melittin in bilayers of 7:3 DOPC/DOPG ratio. For clarity, only two spectra of the P/L (1:20 and 1:40) are shown. The reference I and S spectra were obtained from melittin in dimyristoyl phosphatidylcholine bilayers (2). Each spectrum from the DOPC/DOPG mixture was fit by a linear superposition of S and I spectra (dotted lines). The fraction in I represents the fraction of melittin helices oriented normal to the plane of the membrane (Fig. 2).

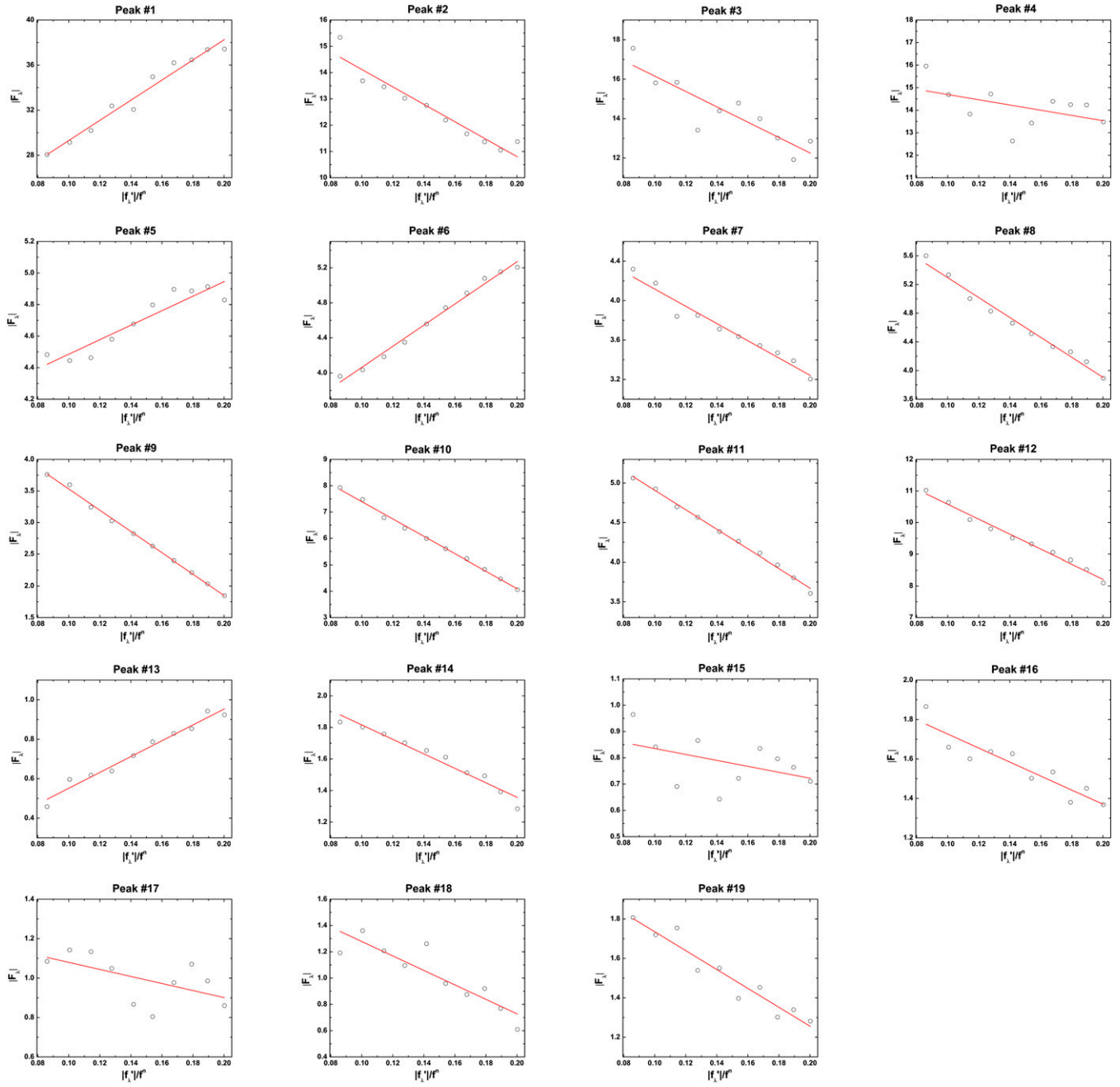

Fig. S4. Multiwavelength anomalous dispersion (MAD) analyses for the detected peaks. For each independent peak, the square root of the integrated intensity, $|F_\lambda|$, is plotted as a function of $|f'_\lambda|/f''$. The data are fit with a straight line, from which $|F_0|$, $|F_2|$, and the ratio F_0/F_2 are obtained. The results are shown in Table S2.

Table S1. Data for the 10 runs of the GUV experiment

Run no.	1	2	3	4	5	6	7	8	9	10	Average	σ
($\Delta A/A$)*, %	4.51	2.81	3.29	3.01	3.48	3.69	3.55	3.01	3.05	3.37	3.38	0.49
Melittin conc., μM	2	1	1	1	5	1	0.75	1	1	1		

($\Delta A/A$)* is the value of the fractional membrane area expansion at the onset of molecular leakage from the GUV. Runs 1–5 used FITC-melittin. Runs 6–10 used melittin. σ is the SD. (The average of runs 1–5 is 3.42 ± 0.59%.)

Table S2. Data for the unit cell reconstruction

No.	(*H,K,L*)	$\lvert F_2\rvert$	$\lvert F_0\rvert$	$-F_0/F_2$	*r*	F_2 phase
1	(0,0,3)	89.41	20.37	0.228	0.963	+
2	(0,0,6)	33.16	17.44	−0.526	0.914	−
3	(0,0,9)	38.94	20.05	−0.515	0.765	−
4	(0,0,12)	11.61	15.86	−1.366	0.155	−
5	(1,0,1)(−1,1,1)(0,−1,1)	4.60	4.03	0.875	0.850	−
6	(0,1,2)(−1,0,2)(1,−1,2)	12.05	2.86	0.237	0.988	−
7	(1,0,4)(−1,1,4)(0,−1,4)	8.74	4.99	−0.571	0.955	+
8	(0,1,5)(−1,0,5)(1,−1,5)	13.90	6.69	−0.481	0.981	+
9	(1,0,7)(−1,1,7)(0,−1,7)	16.81	5.21	−0.310	0.997	−
10	(0,1,8)(−1,0,8)(1,−1,8)	32.97	10.69	−0.324	0.996	+
11	(1,0,10)(−1,1,10)(0,−1,10)	12.36	6.15	−0.497	0.995	−
12	(0,1,11)(−1,0,11)(1,−1,11)	23.69	12.95	−0.547	0.986	+
13	(1,1,3)(−1,2,3)(−2,1,3)(−1,−1,3)(1,−2,3)(2,−1,3)	4.01	0.15	0.037	0.968	−
14	(1,1,9)(−1,2,9)(−2,1,9)(−1,−1,9)(1,−2,9)(2,−1,9)	4.59	2.28	−0.496	0.954	−
15	(1,1,12)(−1,2,12)(−2,1,12)(−1,−1,12)(1,−2,12)(2,−1,12)	1.13	0.95	−0.839	0.106	+
16	(0,2,1)(−2,0,1)(2,−2,1)	3.55	2.08	−0.587	0.833	−
17	(2,0,2)(−2,2,2)(0,−2,2)	1.79	1.26	−0.705	0.249	−
18	(2,0,8)(−2,2,8)(0,−2,8)	5.50	1.83	−0.332	0.775	−
19	(0,2,10)(−2,0,10)(2,−2,10)	4.79	2.21	−0.462	0.916	−

Results of multiwavelength anomalous dispersion analysis. Nineteen independent diffraction peaks, denoted by crystal indices (*H,K,L*), were detected. $\lvert F_2\rvert$, $\lvert F_0\rvert$, and $-F_0/F_2$ were obtained from the linear fits shown in Fig. S4, and *r* is the correlation coefficient of the linear fit.

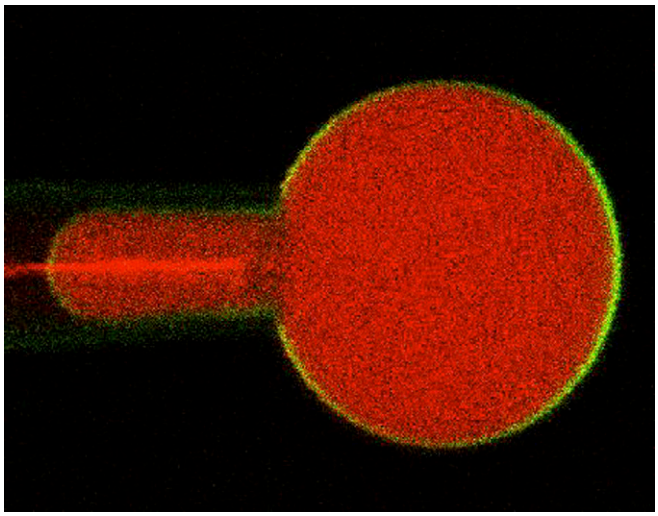

Movie S1. In this movie of Fig. 1, the red line on the micropipette is an optical artifact. At the beginning, the GUV with a DOPC/DOPG ratio of 7:3 is seen by the red color of the soluble dye Texas red sulfonyl chloride (TRsc) (625 M_r, 10 μM inside the GUV). The green color on the surface of the GUV indicates the binding of FITC-melittin (2 μM outside the GUV). The binding causes the area expansion; hence, the protrusion in the micropipette increases. Then, the intensity of the red color suddenly begins to decrease and diminish, indicating the formation of stable pores in the membrane. For awhile, the protrusion length continues to increase due to further binding of melittin. As explained in *SI Text, Giant Unilamellar Vesicle Protrusion*, the formation of stable pores causes the GUV to swell because of our initial preparation with sucrose inside vs. glucose outside the GUV. After the melittin binding reaches equilibrium, the protrusion length eventually decreases due to the GUV volume increase. The real time of the movie is 400 s in total. Photobleaching was negligible.

Movie S1